Dalton Transactions

ROYAL SOCIETY OF CHEMISTRY

PAPER

View Article Online
View Journal | View Issue

Cite this: *Dalton Trans.*, 2025, **54**, 5486

The family of tetranuclear Nb_4OI_{12-x} clusters (x = 0, 1, 2): from the molecular Nb_4OI_{12} cluster to extended chains and layers†

Jan Beitlberger, [a] Mario Martin, [b] Marcus Scheele, [b] Patrick Schmidt, [a] Markus Ströbele [a] and H.-Jürgen Meyer *[a]

Received 21st January 2025,
Accepted 26th February 2025

DOI: 10.1039/d5dt00174a

rsc.li/dalton

Unconventional reduction reactions in the Nb–O–I system have produced a number of niobium oxyiodides containing the oxygen-centered [Nb_4O] cluster. Crystalline Nb_4OI_{12} and two modifications of Nb_4OI_{11} were structurally characterized by means of single-crystal X-ray diffraction studies. The new compounds can be classified as members of the Nb_4OI_{12-x} family, together with the already known Nb_4OI_{10}. Nb_4OI_{12} is represented by a molecular stucture, in which the two modifications of Nb_4OI_{11} are forming structures with iodido-bridged strings, that can be assigned to represent one-dimensional structures. Measurements of b-Nb_4OI_{11} single crystals reveal semiconducting behaviour, with an electrical conductivity in the order of 10^{-3} S m^{-1} at 300 K and an electrical band gap estimated as 0.4 eV. The presence of varying numbers of cluster electrons in the given compounds is discussed in the light of second-order Jahn–Teller distortion.

Introduction

Metal clusters display a broad variety in structural arrangements and oxidation states. A large number of transition metal (M) halide (X) clusters have been reported with the octahedral [M_6] cluster core, being represented with [M_6X_{12}]- and [M_6X_8]-type architectures.[1] The [M_6X_{12}]-type constitutes an octahedral M_6 cluster with twelve X atoms capping all edges of the M_6 core and is typically obtained for combinations of larger M and smaller X atoms. The [M_6X_8] cluster constitutes an octahedral cluster with eight face-capping ligands of the M_6 cluster and is typically obtained for combinations of smaller M and larger X atoms. The well-known niobium cluster compounds Nb_6Cl_{14} and Nb_6I_{11} are good examples of these two architectures, of which the latter can be described as $(Nb_6I^i_8)I^{a-a}{}_{6/2}$ (i = innen or inner; a = außen or outer), emphasizing the presence of an [M_6X_8] cluster and a connectivity pattern in which six outer iodide ligands are shared between two clusters.[2,3]

The connectivity between adjacent cluster cores and the number of cluster electrons being present has an important impact on the electronic properties of cluster compounds. A connectivity, where inner ligands simultaneously act as outer ones (i–a and a–i connectivity), is obtained in Chevrel phases like $PbMo_6S_8$, which is showing superconducting properties as a result of metal-to-metal interactions between adjacent clusters.[4]

A successive dimensional reduction of cluster connectivities is exemplified when going from Nb_6I_{11} [$(Nb_6I^i_8)I^{a-a}{}_{6/2}$] having six shared outer ligands in three dimensions, along to W_6I_{12} [$(W_6I_8{}^i)I^a{}_2I^{a-a}{}_{4/2}$] having four bridging apical ligands, creating layers, and finally to BiW_6Cl_{15} [$BiCl_2(W_6Cl^i_8)Cl^a{}_4Cl^{a-a}{}_{2/2}$] with two bridging apical ligands, creating a linear arrangement of clusters.[3,5] Isolated clusters like W_6Cl_{18} ($(W_6Cl^i_8)Cl^a_6$) are held together by van der Waals forces.[6]

Metal-rich niobium iodides involve the compounds Nb_6I_{11}, Nb_3I_8, NbI_3, and NbI_4.[3,7] A promising approach for the expansion of this chemistry is the introduction of another anion to create a heteroanionic metal cluster compound. An early outcome of this approach was the insertion of an interstitial atom (Z) into the octahedral [M_6X_{12}]-type cluster core to yield [M_6ZX_{12}], mostly evident with the electron-poorer d-metals (M = Zr, Hf).[8] The formation of an interstitially stabilized cluster is uncommon for [M_6X_8]-type clusters, obviously due to an unfavorable short distance between the interstitial and the face-capping anion, causing repulsion. An exception is Nb_6I_{11} which can incorporate a hydrogen atom to form the interstitially stabilized compound Nb_6HI_{11}.[9]

[a]*Section for Solid State and Theoretical Inorganic Chemistry Institute of Inorganic Chemistry Auf der Morgenstelle 18, 72076 Tübingen, Germany. E-mail: juergen.meyer@uni-tuebingen.de*
[b]*Institute of Physical and Theoretical Chemistry Auf der Morgenstelle 18, 72076 Tübingen, Germany*

†Electronic supplementary information (ESI) available: IR spectra, X-ray diffraction pattern of b-Nb_4OI_{11}, photographs of crystals. CCDC 2366237, 2391069 and 2408695. For crystallographic data in CIF or other electronic format see DOI: https://doi.org/10.1039/d5dt00174a

Generally, heteroanionic clusters can also be envisioned to constitute anion replacements in given architectures to induce a modified structure or connectivity pattern of clusters, as exemplified for Nb_6I_9S (derived from Nb_6I_{11}), Nb_3X_7S (X = Cl, Br, I) and ANb_3Br_7S with A = Rb, Cs (derived form Nb_3X_8).[10]

The employment of oxide as a heteroanion unavoidably leads to the formation of oxyhalides $NbOI_2$, $NbOI_3$ and NbO_2I.[11] However, it has been demonstrated that new oxyiodide cluster compounds can be obtained under certain conditions. A most recent example of a new oxyiodide cluster is Nb_4OI_{10}, which has been characterized as a small band-gap semiconductor showing photoresponse.[12] Its crystal structure can be easily derived from that of Nb_6I_{11} by cutting-off two $(NbI^{a-a}{}_{1/2})$-groups of $(Nb_6I^{i}{}_8)I^{a-a}{}_{6/2}$. The resulting planar $[(Nb_4OI^{i}{}_8)I^{a-a}{}_{4/2}]$ cluster is allowing the presence of a surplus oxygen atom in the cluster center. The relaxation of inner iodide ligands in this structure is avoiding strong interanionic $O–I^{i}$ repulsions that would likely inhibit an oxygen centering in Nb_6I_{11}.

The preparation of niobium oxyiodide cluster compounds requires subtle control of reaction conditions and can otherwise lead to the crystallization of the thermodynamic more stable known niobium oxyiodides. Such conditions involve a highly dynamic system including elusive phases whose equilibria depend on the temperature and on local concentrations, as has been previously demonstrated with the newly discovered compound $W_2O_3I_4$ in the W–O–I system.[13] By varying the synthetic conditions, we herein describe the crystal structures of three tetranuclear niobium cluster compounds that we have characterized in the Nb–O–I system. The previously reported Nb_4OI_{10} and the herein described compounds are represented by a $[Nb_4O]$ cluster core that is interconnected in different ways following a dimensional reduction from layers (Nb_4OI_{10}) over strings (Nb_4OI_{11}) to isolated molecules (Nb_4OI_{12}).

Results and discussion

Synthesis and crystal structure

Recently, we have described the new cluster compound Nb_4OI_{10} whose structure is based on a rectangular $[Nb_4O]$ core that is interconnected into layers by iodide ligands.[12] The crystal structure features a two-dimensional van der Waals material representing a small band gap semiconductor.

Slight variations of the synthesis conditions relative to those given for Nb_4OI_{10} revealed the existence of a number of related compounds to exist in the Nb–O–I system. These compounds are generated by changing the concentrations of reaction partners and by subtle variations of the temperature program of reactions. For a general understanding of this type of reaction we have to consider the chemical changes that occur on heating solid reactants in a heterogeneous solid-state reaction with the involvement of solid and gaseous phases. This has been already exemplified by the formation of niobium oxyiodides ($NbOI_2$, $NbOI_3$ and NbO_2I) that were described previously.[11] For the preparation of reduced compounds in the Nb–O–I system, we are avoiding the classical pathway of a metallothermic reduction. Instead, we are exploring unconventional reduction agents with the employment of the carbodiimide ion $(N{=}C{=}N)^{2-}$.

At elevated temperatures, carbodiimides have the tendency to decompose and to act as reducing agents. In this process, metal ions can be reduced, some even to form the metal state.[14] The decomposition product of carbodiimide in such a reaction is not fully evidenced, as products appear X-ray amorphous. However, infrared spectra indicate the formation of C_3N_4 (Fig. S1 and S2†).[15] A corresponding reduction mechanism could follow reaction (1).

$$3\,CN_2{}^{2-} \xrightarrow{\Delta T} C_3N_4 + N_2 + 2e^- \quad (1)$$

All three compounds reported in this work crystalize as black, block-like crystals (Fig. 1). They were investigated by X-ray powder and single-crystal diffraction, providing X-ray intensity data for subsequent crystal structure determinations. The crystallographic data and refinement parameters of all tetranuclear cluster compounds are summarized in Table 1.

Syntheses of the new compounds are performed in evacuated/fused silica tubes at temperatures up to 500 °C. Nb_4OI_{12} and b-Nb_4OI_{11} were prepared from $NbI_4 : Li_2(CN_2) : Li_2O$ mixtures with 4 : 1 : 1 and 4 : 1.5 : 1 molar proportions, respectively. a-Nb_4OI_{11} was synthesized by a reaction mixture of $NbI_4 : K_2CN_2 : Cu_2O$ in 4 : 1.5 : 1 molar ratio (see Experimental section for more details).

The Nb_4OI_{12-x} system includes four structures with sum formulae Nb_4OI_{12}, Nb_4OI_{11}, and Nb_4OI_{10}. Nb_4OI_{11} appears with two modifications, denoted as “a” and “b”.

The parent compound Nb_4OI_{12} features a molecular structure based on the rectangular $[Nb_4O]$ cluster core with eight (μ_2-) capping and four terminal iodide atoms, shown in Fig. 2. The unit cell contains eight molecules that interact through

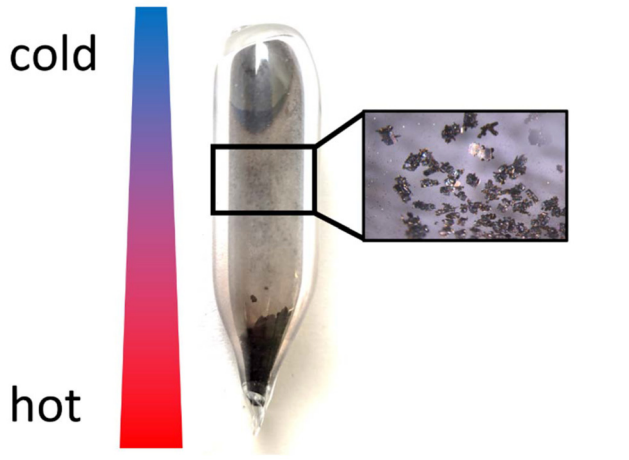

Fig. 1 A typical ampoule after the reaction is performed. The temperature gradient during the reaction is illustrated through the bar on the left side (red: hot region, blue cold region). The inset shows the reaction product b-Nb_4OI_{11} (see also Fig. S4†).

Table 1 Crystal data and structure refinement parameters of Nb_4OI_{12-x} compounds

	Nb_4OI_{12}	a-Nb_4OI_{11}	b-Nb_4OI_{11}	Nb_4OI_{10} [12]
CCDC no.	2366237	2391069	2408695	2225618
Space group	$Pmc2_1$	$C2/m$	$P\bar{1}$	$P2_1/n$
Temperature (K)	270	220	150	150
Unit cell dimensions	a = 37.9189(8) Å	a = 15.4442(3) Å	a = 10.1217(2) Å	a = 10.0435(1) Å
	b = 17.8026(4) Å	b = 13.0449(2) Å	b = 13.9844(3) Å	b = 10.6595(1) Å
	c = 7.3403(2) Å	c = 11.9078(2) Å	c = 16.3913(3) Å	c = 10.0594(1) Å
	α = 90°	α = 90°	α = 88.968(2)°	α = 90°
	β = 90°	β = 105.698(2)°	β = 89.093(2)°	β = 94.193(1)°
	γ = 90°	γ = 90°	γ = 85.329(2)°	γ = 90°
Volume (Å^3)	4955.1(2)	2309.56(7)	2311.80(8)	1074.06(2)
Z	8	4	2	2
Wavelength (Å)	0.71073	0.71073	0.71073	0.71073
μ (mm^{-1})	16.744	16.624	16.607	16.433
2θ range for data collection	4.576 to 50.700	4.154 to 57.396	7.186 to 76.742	5.532 to 72.638
Total number of reflections	53 804	44 103	17 704	80 092
Independent reflections	9037	3115	17 704	5209
Refined parameters	418	91	290	71
R_{int}	0.0351	0.0189	0.020	0.0354
R_1	0.0517	0.0150	0.0185	0.0117
wR_2	0.1414	0.0314	0.0581	0.0282
Goodness-of-fit on F^2	1.086	1.430	1.037	1.093

van der Waals bonding. The crystal structure measurement was performed near room temperature because low-temperature measurements revealed incoherent scattering patterns, which could be likely indicative for the appearance of a phase-transition.

Three distinct Nb_4OI_{12} molecules are present in the crystal structure. Each of them exhibits a (nearly) rectangular cluster core with six electrons being available for Nb–Nb bonding. The bond lengths of the cluster cores hold a small variability (Fig. 2). The short and the long interatomic distances of the cluster are in the range of 2.793(3)–2.807(3) Å and 3.029(7)–3.051(3) Å, suggesting more electron density in each shorter Nb–Nb contact. Regarding the crystal structure, the Nb_4OI_{12} molecules are arranged in layers along the *ac*- and *bc*-planes (Fig. 3). When looking along the *b* axis (Fig. 3, right), the stacking of the molecules in the *a* direction could be explained as an ABCB sequence, although there is no closest packing of the molecules. The molecules are just arranging to each other in three different *bc*-planes (denoted in Fig. 3 as A, B and C) to reduce repulsion.

When departing from the molecular Nb_4OI_{12} structure, the crystal structure of Nb_4OI_{11} contains one iodide atom less and appears with two modifications. We denote these modifications with "a" and "b" because no conversion from one into the other structure could be discovered experimentally. The structure of a-Nb_4OI_{11} is represented by a string-like connectivity of $(Nb_4OI_8)I_2I_{2/2}$ cluster chains, in which each of the two distinct clusters is iodine bridged in a *trans* connection to the next cluster (Fig. 4). The $[Nb_4O]$ cluster cores in this structure are as well in a rectangular shape, having two short (2.7368(6)–2.7584(7) Å) and two long (3.0375(6)–3.0423(6) Å) Nb–Nb distances.

The presence of Nb2 atoms over all equivalent (8j) positions would create a layered structure with $[Nb_4O]$- and $[Nb_6O]$-cluster cores, shown in Fig. 5. However, the Nb2 positions (highlighted in light blue) are occupied by only $\frac{1}{2}$ resulting in a string connectivity. In fact, this picture (Fig. 5) represents a superposition of the alternating layers in the structure. The crystal structure of a-Nb_4OI_{11} is characterized by two alternating layers of $(Nb_4OI_8)I_2I_{2/2}$ that are stacked on top of each other along the [100] direction. The cluster strings within the alternating layers in the structure, each of them shown in Fig. 6, are running in two different directions ([011] and [01–1]). This arrangement affords an alternating occupation of Nb2 positions in each layer. The adhesion between adjacent strings and layers in the structure can be described as van der Waals type, forming a hexagonal packing of strings.

Another modification of Nb_4OI_{11} is denoted as b-Nb_4OI_{11}. The crystal structure of b-Nb_4OI_{11} again features a string-like connectivity of two distinct $[Nb_4O]$ clusters. However, the connectivity pattern *via* iodine atoms alternates with a *cis* and a *trans* connectivity of $[Nb_4O]$ cores. Each trans connected cluster includes two short and two long Nb–Nb distance within the $[Nb_4O]$ core. The same is true for the *cis* connected cluster. However, the *cis* connectivity induces a significant distortion to the cluster, specified in Table 2.

The unit cell of the crystal structure of b-Nb_4OI_{11} is projected in Fig. 7. In contrast to the bidirectional arrangement of cluster strings in the structure of a-Nb_4OI_{11}, all cluster strings in b-Nb_4OI_{11} are running parallel into one direction ([001]). A view on the projected *ab*-plane suggests that the separate strings are hold together by van der Waals interactions. The given arrangement of $(Nb_4OI_8)I_2I_{2/2}$ chains be derived from a hexagonal packing of strings, which is a typical structure pattern observed for one-dimensional structures (Fig. 8).

Electrical conductivity of b-Nb_4OI_{11}

Crystal structures like those of a- and b-Nb_4OI_{11} with one-dimensional connectivities may be expected to act as one-

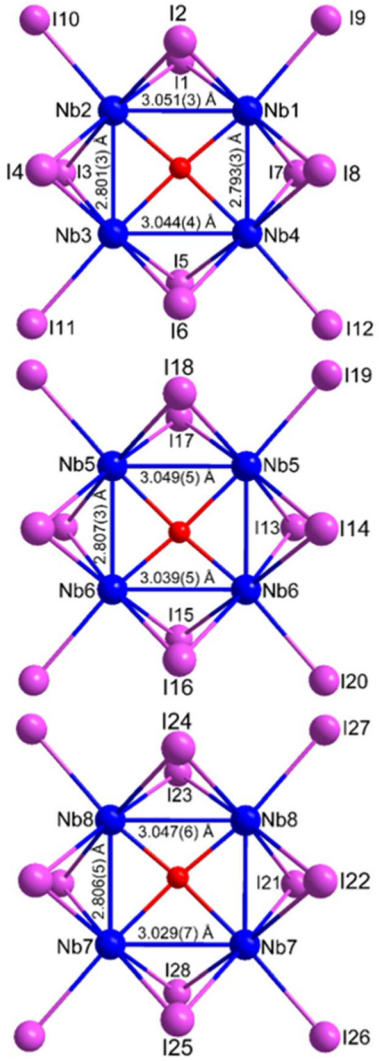

Fig. 2 Three distinct Nb_4OI_{12} molecules with atom labels and Nb–Nb distances given.

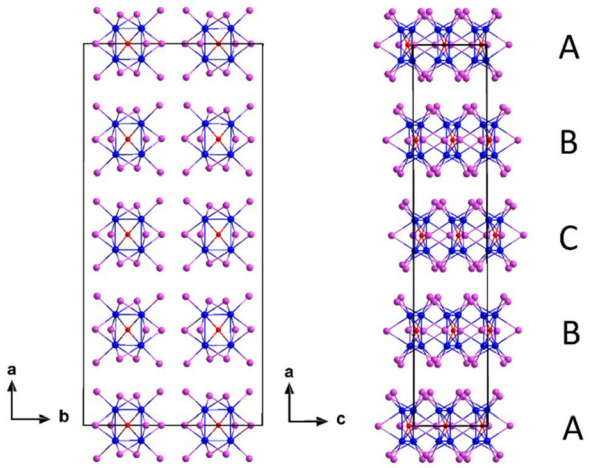

Fig. 3 Section of the crystal structure of Nb_4OI_{12}, looking along the *c*- and *b*-axis. Niobium atoms are coloured in blue, iodine in pink, and oxygen in red.

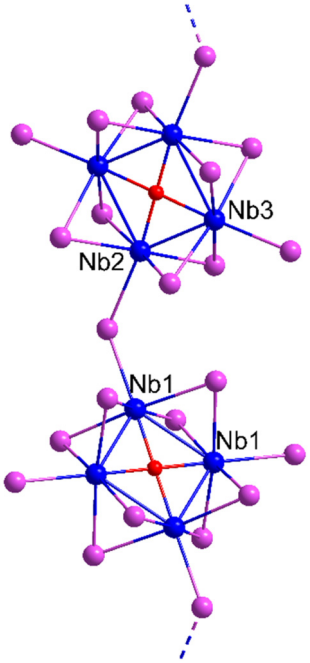

Fig. 4 String-like connectivity in the structure of a-Nb_4OI_{11}.

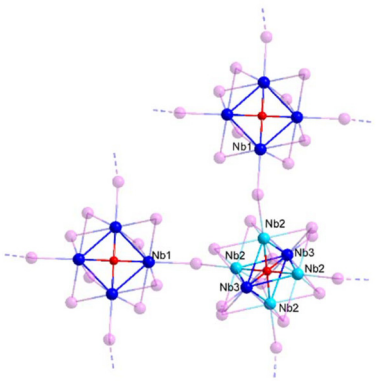

Fig. 5 Cluster connectivity in the structure of a-Nb_4OI_{11} with the equivalent Nb2 positions coloured in cyan. Due to the half-occupation of Nb2 sites, only one pair of Nb2 atoms is present.

dimensional conductors. Hence, the electrical conductivity properties of single crystals of b-Nb_4OI_{11} where investigated.

In Fig. 9, we display a two-point probe *I*–*U* sweep of a typical rod-shaped b-Nb_4OI_{11} crystal from which we calculate the electrical conductivity as $\sigma = 4.5 \times 10^{-3}$ S m^{-1} at 300 K.[16,17]

The temperature-dependent conductivity measurement in Fig. 10 indicates an Arrhenius-type, temperature-activated transport, which is typical for semiconducting materials.[12,17,18]

From this plot, we obtain an activation energy of E_A = 0.2 eV. Thus, in a first-order approximation the energy difference of the Fermi level to the conduction band can be gauged as 0.2 eV. Under the assumption of an intrinsic position of the fermi

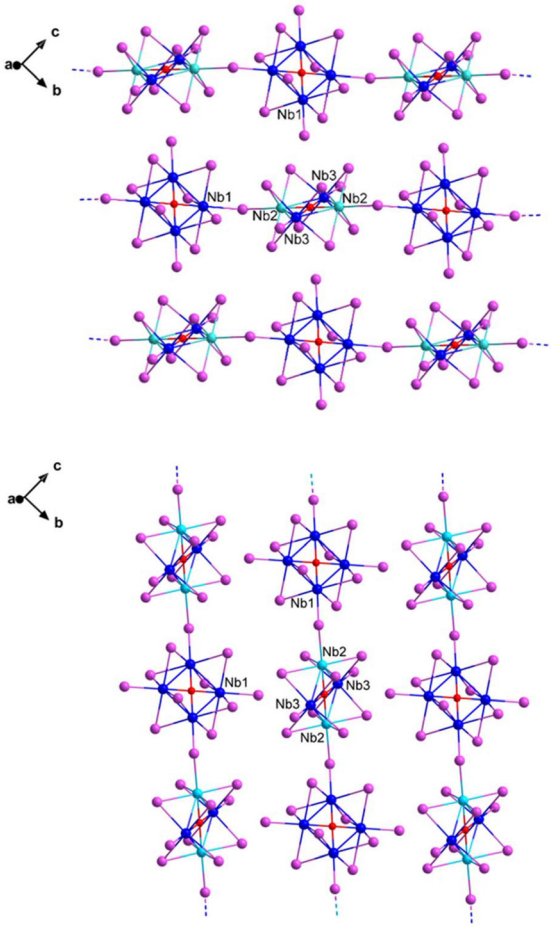

Fig. 6 Arrangement of individual cluster layers in the structure, based on string-like connectivities in the structure of a-Nb_4OI_{11}.

level, this would suggest an electrical band gap on the order of 0.4 eV.

The photoresponse at 300 K of b-Nb_4OI_{11} toward optical excitation with a 779 nm laser in continuous wave mode is shown in Fig. 11. An initial fast photocurrent of ~65 nA is followed by a slower, second component under continuous excitation. We attribute this slow component to thermal excitation by heating the crystal with the laser. At lower temperature, the photocurrent decreases substantially, *e.g.* to 12.6 pA at 160 K.

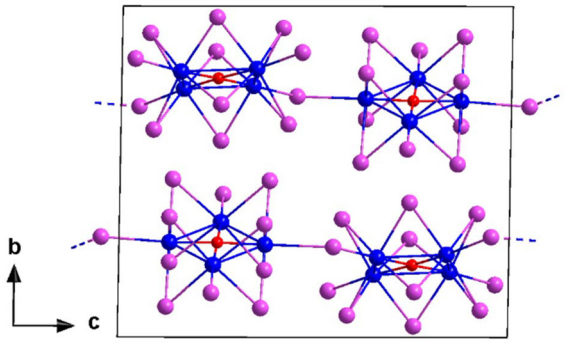

Fig. 7 Section of the crystal structure of b-Nb_4OI_{11}, looking along [100].

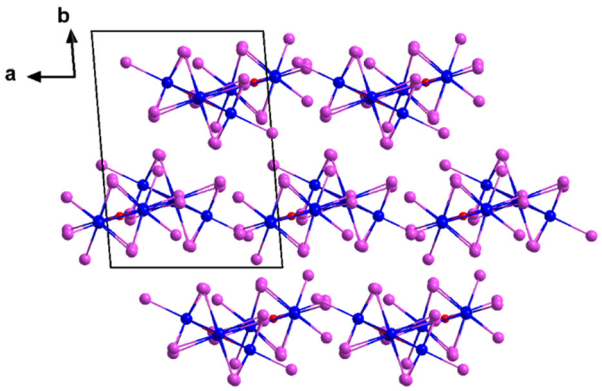

Fig. 8 Section of the crystal structure of b-Nb_4OI_{11}, following the [001] string direction.

Electronic properties of Nb_4OI_{12-x} compounds

One member of the Nb_4OI_{12-x} family was already described before as Nb_4OI_{10}.[12] Nb_4OI_{10} appears with black, plate-like crystals with an electronic band gap near 0.4 eV, according to an experimental bandgap determination and band structure calculation. This compound contains $(Nb_4OI_8)I_{4/2}$ units that are connected into layers, through four shared apical iodide atoms (Fig. 12). The cluster core itself is rectangular with Nb–Nb distances of 2.6232(2) Å and 3.1042(2) Å. This compound was reported with an electrical conductivity of $\sigma \approx 1$ S m^{-1} at 300 K.

Table 2 The Nb_4OI_{12-x} family with the respective number of cluster electrons of each compound, interatomic distances with average values (Ø) and distance ranges along the short and long cluster edges, and angles within the [Nb_4O] cluster core

Distances and angles	Nb_4OI_{12} 6 cluster-e$^-$	a-Nb_4OI_{11} 7 cluster-e$^-$	b-Nb_4OI_{11} (*trans*) 7 cluster-e$^-$	b-Nb_4OI_{11} (*cis*) 7 cluster-e$^-$	Nb_4OI_{10} [12] 8 cluster-e$^-$
short Nb–Nb (Å)	Ø 2.802	Ø 2.748	Ø 2.735	Ø 2.729	
	2.793(3)–2.807(3)	2.7368(6)–2.7584(7)	2.7329(8)–2.7369(8)	2.7288(8)–2.7299(8)	2.6232(2)
long Nb–Nb (Å)	Ø 3.044	Ø 3.040	Ø 3.054	Ø 3.056	
	3.029(7)–3.051(3)	3.0375(6)–3.0423(6)	3.0423(8)–3.0656(8)	2.9168(7)–3.1950(8)	3.1042(2)
small Nb–Nb–Nb (°)	89.81(9)–89.93(9)	87.47(2)	87.34(2)–87.88(2)	87.01(2)–87.14(2)	89.568(6)
large Nb–Nb–Nb (°)	90.11(8)–90.23(9)	92.53(1)	92.17(2)–92.60(2)	92.87(2)–92.97(2)	90.431(6)

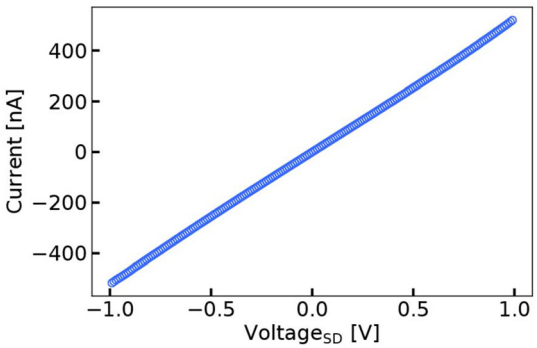

Fig. 9 *I*–*U* sweep in the dark of b-Nb_4OI_{11} at 300 K.

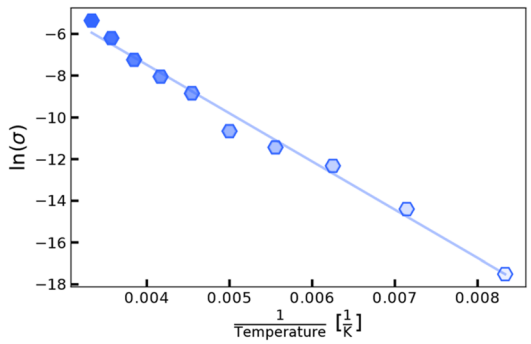

Fig. 10 Arrhenius plot of the electrical conductivity of b-Nb_4OI_{11}, with 20 K temperature steps between 120–300 K. The blue line represents a linear Arrhenius fit to the data.

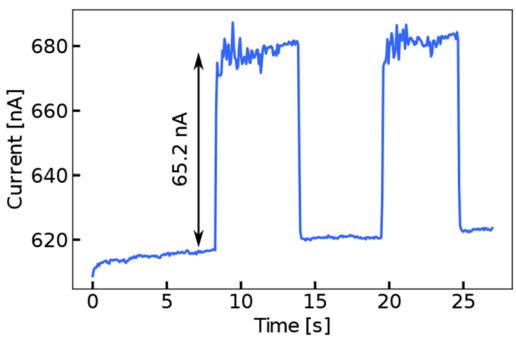

Fig. 11 Photoresponse of b-Nb_4OI_{11} at 300 K toward a 779 nm laser illumination with 1 V bias applied.

Beside their different connectivities, the cluster compounds of the Nb_4OI_{12-x} family differ not only in their Nb–Nb bond lengths and Nb–Nb–Nb angles, but also by their numbers of cluster electrons, as summarized in Table 2.[12]

From Nb_4OI_{12} to Nb_4OI_{10} there is a difference of two electrons being available for niobium-to-niobium bonding. All compounds are forming nearly rectangular [Nb_4O] clusters in which the longer edges possess almost the same Nb–Nb distances (see Table 2). For the example of Nb_4OI_{10} we already discussed the higher stability of a rectangular *versus* a square cluster core. The resulting symmetry lowering goes along with

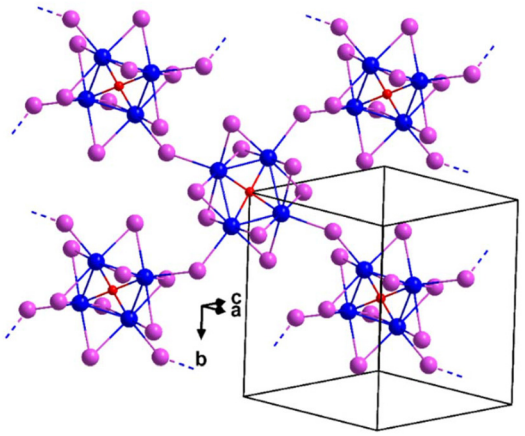

Fig. 12 Visualization of the connectivity of Nb_4OI_{10}.[12]

an increase in hybridization of molecular orbitals through a second-order Jahn–Teller distortion. In other words, the series of compounds are showing higher electron localization within the two shorter edges of [Nb_4O] cluster cores. The rectangular niobium arrangement hosts six electrons for Nb_4OI_{12}, seven electrons for Nb_4OI_{11}, and eight electrons for Nb_4OI_{10}, thereby undergoing a continuous shrinkage of the short Nb–Nb distance, with the values given in Table 2.

If there were less than six electrons for Nb–Nb bonding, the bond lengths should elongate even more. Such a compound is not yet known in the Nb–O–I system. However, the structure of $Nb_4OTe_9I_4$ contains an oxygen centered Nb_4 cluster core having four cluster electrons for Nb–Nb bonding.[19] The cluster is distorted into a flattened tetrahedral shape with nearly equal Nb–Nb distances of 3.057(4) Å and 3.050(3) Å. These are quite close to the long distances present in the [Nb_4O] cluster cores presented in this work.

Conclusion

Cluster compounds can show a broad flexibility in their oxidation states. A well-established example is the binary tungsten-iodide system, with more than 20 different structures being reported.[20] The addition of oxygen leads into the W–O–I system, that is well-known because WO_2I_2 is a prominent compound in chemical vapor transport (CVT) reactions.[13] The thermal treatment of WO_2I_2 leads to $W_2O_3I_4$ first, and then to WO_2. All oxides and oxyiodides in this system appear under discrete temperature conditions.

An even broader chemistry is now discovered in the Nb–O–I system for Nb_4OI_{12-x} (x = 0, 1, 2) compounds, with their rectangular [Nb_4O] cluster cores appearing in layers, strings, and in isolated molecules. The distinct connectivity patterns in the crystal structures involve different semiconducting properties.

These compounds could not be prepared in conventional reduction attempts through metallothermic reduction. In contrast, comparably soft reduction conditions were successful, with the carbodiimide ion as reducing agent. Hence, the formation of compounds in the Nb–O–I system involves uncon-

ventional reduction reactions in heterogeneous solid-state reactions. The product formation involves subtle equilibrium conditions related to small changes in temperature and local concentrations. These conditions appear fairly complex and are further complicated by other new compounds that exist in the given Nb–O–I system besides the herein described tetranuclear cluster compounds. The discovery of compounds with pentanuclear and heptanuclear niobium clusters in the Nb–O–I system will be reported shortly.

Experimental section

Materials and methods

Manipulations of starting materials and products were performed in a glovebox under dry argon with moisture and oxygen levels below 1 ppm. Reaction partners were charged into silica tubes ($V \approx 1.5$ cm^3). Li_2O (ABCR, 95%) and Cu_2O (Sigma-Aldrich, 99.99%) were used as purchased. NbI_4, $Li_2(CN_2)$ and $K_2(CN_2)$ were synthesized as described in the literature.[21] Nb_4OI_{10} was synthesized as described before.[12]

Syntheses

b-Nb_4OI_{11} and Nb_4OI_{12} were synthesized from NbI_4, Li_2O and $Li_2(CN_2)$. For this purpose, NbI_4 (160.8 mg, 0.268 mmol), Li_2O (2 mg, 0.067 mmol), and $Li_2(CN_2)$ (5.4 mg, 0.101 mmol (b-Nb_4OI_{11}) or 3.6 mg, 0.067 mmol (Nb_4OI_{12})) were encapsulated into fused silica ampoules. The ampoules were heated from room temperature to 500 °C with a rate of 0.1 °C min^{-1}. The holding time was 24 h before the reactions were allowed to cool to room temperature with a rate of 5 °C min^{-1} for b-Nb_4OI_{11} and a rate of 10 °C min^{-1} for Nb_4OI_{12}. Block-like crystals of b-Nb_4OI_{11} and Nb_4OI_{12} were found on the wall of the ampoule, along with some $NbOI_2$ and NbI_5 at the top of the ampoule. The products were collected mechanically. The compounds are sensitive to moisture. A powder XRD pattern of b-Nb_4OI_{11} is shown in Fig. S3.† Examples of crystal specimens of b-Nb_4OI_{11} and Nb_4OI_{12} can be seen in Fig. S4 and S5.†

a-Nb_4OI_{11} was synthesized from NbI_4, Cu_2O and $K_2(CN_2)$. For this purpose, NbI_4 (100.7 mg, 0.168 mmol), Cu_2O (6 mg, 0.042 mmol), and $K_2(CN_2)$ (7.4 mg, 0.063 mmol) were encapsulated into a fused silica ampoule. The ampoule was heated from room temperature to 500 °C with a rate of 0.1 °C min^{-1}. The holding time was 24 h before the reaction was allowed to cool to room temperature with a rate of 5 °C min^{-1}. Block-like crystals of a-Nb_4OI_{11} were found on the wall of the ampoule, along with some $NbOI_2$ and NbI_5 at the top of the ampoule. The product was collected mechanically. The compound is sensitive to moisture.

Instrumentation

X-ray diffraction

Black block-shaped single-crystals of a-Nb_4OI_{11}, b-Nb_4OI_{11}, and Nb_4OI_{12} were mounted on a Rigaku XtaLab Synergy-S X-ray diffractometer using Mo-K_α (λ = 0.71073 Å) radiation. The single-crystal was kept under N_2 cooling at 270 K for Nb_4OI_{12}, at 220 K for a-Nb_4OI_{11} and at 150 K for b-Nb_4OI_{11} during the data collection. Corrections for absorption effects were applied with CrysAlisPro (Rigaku Oxford Diffraction, 2020). The crystal structure was solved by the integrated space group and crystal structure determination routine of ShelXT[22] and refined by full-matrix least-squares refinement with ShelXL–2019/3[22] implemented in Olex2.[23]

Reaction products were investigated by powder X-ray diffraction (PXRD) using a StadiP diffractometer (Stoe, Darmstadt) with Ge[111]-monochromated Cu-$K_{\alpha1}$ radiation and a mythen1 detector.

Electrical conductivity

Conductivity measurements were performed in a Lake Shore Cryotronics CRX–6.5 K probe station with a Keithley 2636B source meter unit. Block-shaped b-Nb_4OI_{11} crystals were contacted with silver paste on a silicon substrate with 770 nm oxide layer and transferred into the chamber under protective gas. The conductive silver pads at each end of the crystals were connected to the circuit with tungsten tips. The chamber was kept under vacuum ($<5 \times 10^{-5}$ mbar) with 20 K temperature steps between 120 K and 300 K during the measurements. Two–point conductivity measurements were performed by varying the applied source–drain voltage from −1 V to 1 V while detecting the current. For time–resolved photocurrent measurements, using a picosecond pulsed laser driver (Taiko PDL M1, PicoQuant) together with a 779 nm laser head (pulse length <500 ps) the crystals were illuminated at 40 mW laser output power using the continuous wave mode under a constant bias of 1 V.

Data availability

Crystallographic data have been deposited at the CCDC under 2366237 (Nb_4OI_{12}), 2391069 (a-Nb_4OI_{11}), and 2408695 (b-Nb_4OI_{11}).†

Data are available within the article.

The data that support the findings of this study are available on request from the corresponding author, H.-J. Meyer.

Conflicts of interest

The authors declare no conflict of interest.

Acknowledgements

This research was supported by the Deutsche Forschungsgemeinschaft (ME 914–32/1 and SCHE1905/9-1).

References

1 L. Pauling, *The Nature of the Chemical Bond and the Structure of Molecules and Crystals: An Introduction to Modern Structural Chemistry*, Cornell University Press, 1960.

2 A. Simon, H. G. von Schnering, H. Wöhrle and H. Schäfer, *Z. Anorg. Allg. Chem.*, 1965, **339**, 155–170.
3 A. Simon, H. G. von Schnering and H. Schäufer, *Z. Anorg. Allg. Chem.*, 1967, **355**, 295–310.
4 O. Peña, *Phys. C*, 2015, **514**, 95–112.
5 M. Ströbele and H.-J. Meyer, *Z. Anorg. Allg. Chem.*, 2009, **635**, 1517–1519; M. Ströbele and H.-J. Meyer, *Inorg. Chem.*, 2017, **56**, 5880–5884.
6 R. Siepmann, H. G. von Schnering and H. Schäfer, *Angew. Chem.*, 1967, **79**, 650–650.
7 A. Simon and H. G. Von Schnering, *J. Less-Common Met.*, 1966, **11**, 31–46; L. F. Dahl and D. L. Wampler, *Acta Crystallogr.*, 1962, **15**, 903–911; P. W. Seabaugh and J. D. Corbett, *Inorg. Chem.*, 1965, **4**, 176–181.
8 R. P. Ziebarth and J. D. Corbett, *J. Less-Common Met.*, 1988, **137**, 21–34; R. P. Ziebarth and J. D. Corbett, *J. Solid State Chem.*, 1989, **80**, 56–67; J. Zhang and J. D. Corbett, *J. Solid State Chem.*, 1994, **109**, 265–271; J. Zhang and J. D. Corbett, *Inorg. Chem.*, 1991, **30**, 431–435; J. D. Smith and J. D. Corbett, *J. Am. Chem. Soc.*, 1984, **106**, 4618–4619; R.-Y. Qi and J. D. Corbett, *Inorg. Chem.*, 1994, **33**, 5727–5732.
9 A. Simon, *Z. Anorg. Allg. Chem.*, 1967, **355**, 311–322.
10 H.-J. Meyer and J. D. Corbett, *Inorg. Chem.*, 1991, **30**, 963–967; P. J. Schmidt and G. Thiele, *Acta Crystallogr., Sect. C: Cryst. Struct. Commun.*, 1997, **53**, 1743–1745; G. V. Khvorykh, A. V. Shevelkov, V. A. Dolgikh and B. A. Popovkin, *J. Solid State Chem.*, 1995, **120**, 311–315; C. M. Pasco, *Electronic and Magnetic Properties of layered Two-Dimensional Materials*, Johns Hopkins University, 2021; F. Grahlow, F. Strauß, M. Scheele, M. Ströbele, A. Carta, S. F. Weber, S. Kroeker, C. P. Romao and H.-J. Meyer, *Phys. Chem. Chem. Phys.*, 2024, **26**, 11789–11797; H.-J. Meyer, *Z. Anorg. Allg. Chem.*, 1994, **620**, 863–866.
11 J. Rijnsdorp and F. Jellinek, *J. Less-Common Met.*, 1978, **61**, 79–82; S. Hartwig, Dissertation, Fakultät für Biologie, Chemie und Geowissenschaften, Bayreuth 2003.
12 J. Beitlberger, M. Ströbele, F. Strauß, M. Scheele, C. P. Romao and H.-J. Meyer, *Eur. J. Inorg. Chem.*, 2024, e202400329.
13 M. Löber, M. Ströbele, C. P. Romao and H.-J. Meyer, *Dalton Trans.*, 2021, **50**, 6789–6792.
14 K. Gibson, M. Ströbele, B. Blaschkowski, J. Glaser, M. Weisser, R. Srinivasan, H. J. Kolb and H.-J. Meyer, *Z. Anorg. Allg. Chem.*, 2003, **629**, 1863–1870.
15 H. Zhao, X. Chen, C. Jia, T. Zhou, X. Qu, J. Jian, Y. Xu and T. Zhou, *Mater. Sci. Eng. B*, 2005, **122**, 90–93; H. Li, Y. Jing, X. Ma, T. Liu, L. Yang, B. Liu, S. Yin, Y. Wei and Y. Wang, *RSC Adv.*, 2017, **7**, 8688–8693.
16 F. Fetzer, A. Maier, M. Hodas, O. Geladari, K. Braun, A. J. Meixner, F. Schreiber, A. Schnepf and M. Scheele, *Nat. Commun.*, 2020, **11**, 6188; D. Meschede, *Gerthsen Physik*, Vol. 22, Springer, 2004.
17 F. Grahlow, F. Strauß, P. Schmidt, J. Valenta, M. Ströbele, M. Scheele, C. P. Romao and H.-J. Meyer, *Inorg. Chem.*, 2024, **63**, 19717–19727.
18 M. M. A. Imran and O. A. Lafi, *Phys. B*, 2013, **410**, 201–205; A. M. Al-Fa'ouri, O. A. Lafi, H. H. Abu-Safe and M. Abu-Kharma, *Arabian J. Chem.*, 2023, **16**, 104535; K. Kiran Kumar, M. Ravi, Y. Pavani, S. Bhavani, A. K. Sharma and V. V. R. Narasimha Rao, *Phys. Rev. B: Condens. Matter Mater. Phys.*, 2011, **406**, 1706–1712; A. S. Hassanien and A. A. Akl, *J. Non-Cryst. Solids*, 2016, **432**, 471–479.
19 W. Tremel, *J. Chem. Soc., Chem. Commun.*, 1992, 709–710.
20 M. Ströbele and H.-J. Meyer, *Dalton Trans.*, 2019, **48**, 1547–1561.
21 G. Brauer, *Handbuch der präparativen anorganischen Chemie*, Enke, 1975; R. Srinivasan, M. Ströbele and H. J. Meyer, *Inorg. Chem.*, 2003, **42**, 3406–3411; M. Ströbele, E. Bayat and H.-J. Meyer, *Inorg. Chem.*, 2024, **63**, 16565–16572.
22 G. Sheldrick, *Acta Crystallogr., Sect. C: Struct. Chem.*, 2015, **71**, 3–8.
23 O. V. Dolomanov, L. J. Bourhis, R. J. Gildea, J. A. K. Howard and H. Puschmann, *J. Appl. Crystallogr.*, 2009, **42**, 339–341.